submitted to *Geophys. J. Int.*

Supplementary material for

A quasi-2D model of dike propagation with non-equilibrium magma crystallization

Rustam Abdullin[1], Oleg Melnik[2]*, Alison Rust[3]

[1]*Novosibirsk State University, Novosibirsk; afaritovich@mail.ru*

[2]*Department of Earth Science, University of Oxford; oleg.melnik@earth.ox.ac.uk*

[3]*School of Earth Science, University of Bristol; Alison.Rust@bristol.ac.uk*

CONTENTS

1 MAGMA PROPERTIES PLOTS

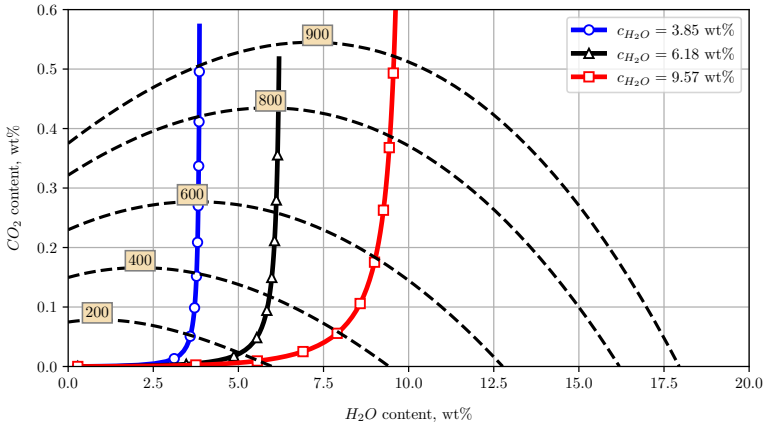

Figure 1. Volatile solubility and degassing paths in a mixed H_2O–CO_2 system computed with the MagmaSat model Ghiorso & Gualda (2015); Iacovino et al. (2021) at 900°C. Dashed lines represent isobars with corresponding pressures labelled in MPa. Coloured solid lines show three closed-system degassing paths starting at 900 MPa with different initial H_2O contents (3.85 wt%, 6.18 wt%, and 9.57 wt%, see legend).

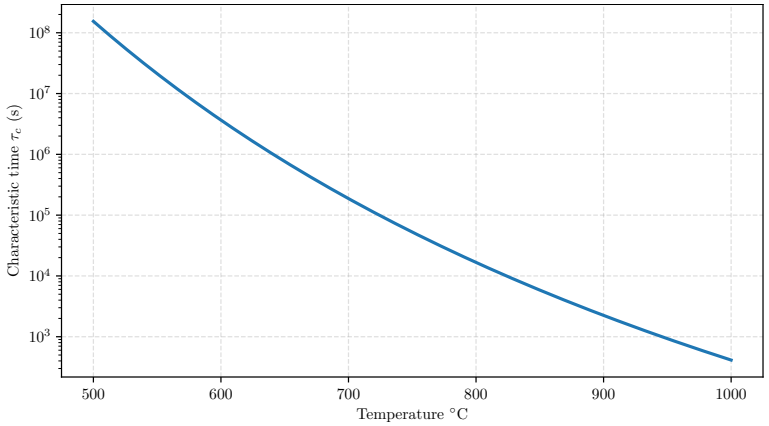

Figure 2. Temperature dependence of the characteristic time scale τ_c governing non-equilibrium crystallization dynamics. The relaxation time is computed using an Arrhenius-type expression $\tau_c = \tau_0 \exp\left(\frac{E}{RT}\right)$ with parameters $\tau_0 = 10^{-6}$ s, $E = 210{,}000$ J/mol, and $R = 8.314$ J/(mol·K). At magmatic conditions above 800°C, the characteristic timescale reduces to hours or less.

2 VERIFICATION

To assess model accuracy, we compare our results with the classical Roper & Lister (2007)Roper & Lister (2007) solution in Figure3. To do this, we assume constant density and viscosity of the magma, and neglect the influence of temperature. The parameters used for validation are given in Table 1. They are chosen to ensure $h_\infty = 1$, $K = 1$, which represent dimensionless far-field half-width and fracture toughness, respectively (see, eq. (2.4), (2.10) in Roper & Lister (2007)). The agreement between the models far from the injection point is very good. The general agreement in dike width and ascent velocity suggests that our numerical approach correctly captures the buoyancy-driven propagation mechanism.

To ensure the reliability of numerical results, a mesh sensitivity analysis was conducted (Figure 4). The plots compare dike front position and ascent velocity for different mesh configurations, varying both the vertical resolution ($\Delta x = 50$ and 100 m) and the number of transverse cells ($N_y = 30$ and 50). The results demonstrate excellent agreement across all cases, indicating that the solution is numerically converged. This confirms that the adopted resolution ($\Delta x = 100$ m, $N_y = 30$) is sufficient to accurately capture the propagation dynamics while maintaining computational efficiency.

Table 1. Simulation parameters for verification with Roper & Lister (2007)

Parameter	Description	Value	Units
E	Young's modulus of the rocks	18.75	GPa
ν	Poisson's ratio of the rocks	0.25	—
ρ_r	Host rock density	2700	kg/m^3
ρ_m	Magma density	2400	kg/m^3
Q_V	Volume source flux per unit width	20	m^2/s
K_{Ic}	Fracture toughness	234	MPa·m$^{1/2}$
g	Gravity acceleration	10	m/s^2
μ	Magma viscosity	100	Pa·s

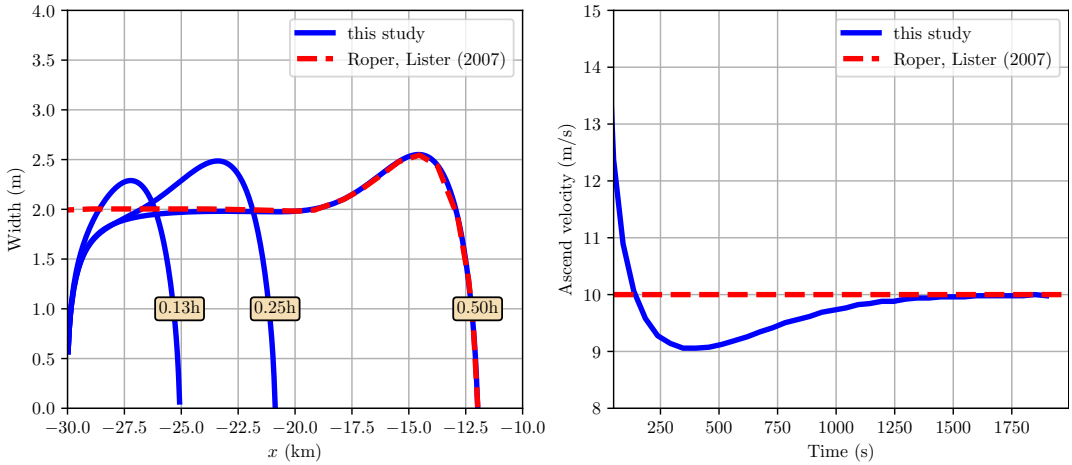

Figure 3. The left panel shows the dike width as a function of depth at different time instants, comparing the results of this study (solid blue line) with the model of Roper & Lister Roper & Lister (2007) (dashed red line). The right panel presents the ascent velocity of magma over time.

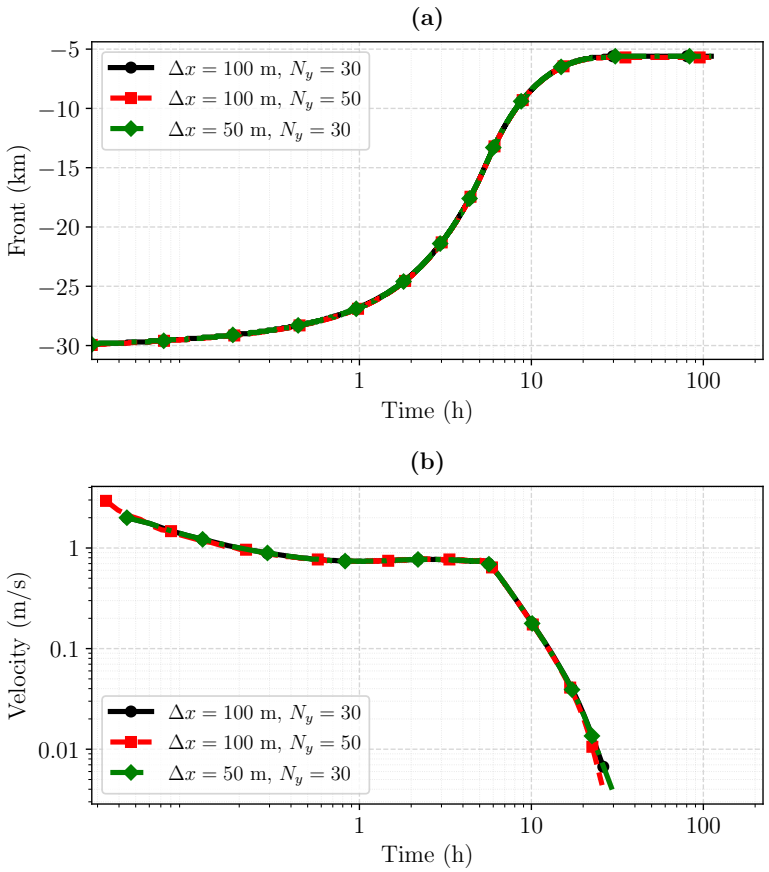

Figure 4. Sensitivity analysis of dike front evolution and ascent velocity with respect to mesh resolution. (a) Dike front position over time. (b) Magma ascent velocity. Results for different spatial resolutions ($\Delta x = 100$ m or 50 m) and transverse mesh densities ($N_y = 30$ or 50) are shown.

3 PARAMETRIC ANALYSIS

To assess the influence of mechanical properties on dike propagation, we conducted a parametric test by varying the Young's modulus of the host rock. Figure 5 presents the front position and ascent velocity for two values of E (20 GPa and 50 GPa). Results indicate that a more compliant host (lower E) slightly facilitates earlier propagation, but does not substantially alter the overall dynamics. This suggests that dike evolution is relatively insensitive to host stiffness within a geologically reasonable range.

We also examined the sensitivity of the model to fracture toughness by comparing three values of K_{Ic}. Figures 6 and 7 show the resulting front position, ascent velocity, and width profiles. Within the tested range, fracture toughness has a negligible effect on dike dynamics, suggesting that thermal and rheological processes dominate the evolution and arrest behavior in this regime.

To better illustrate the contrasting effects of shear heating and latent heat on ascent velocity, we replot the simulation results from Fig. 12 of the main text over a shorter time interval Fig.8

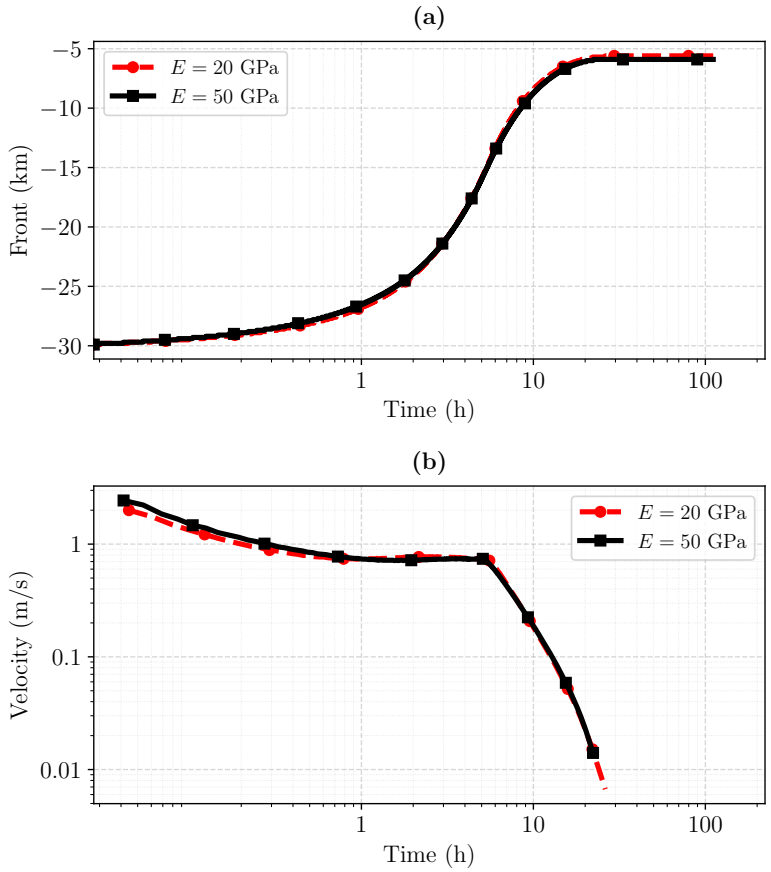

Figure 5. Effect of host rock stiffness on dike propagation. (a) Front position over time for two values of Young's modulus E (20 GPa and 50 GPa). (b) Corresponding ascent velocity on a logarithmic scale.

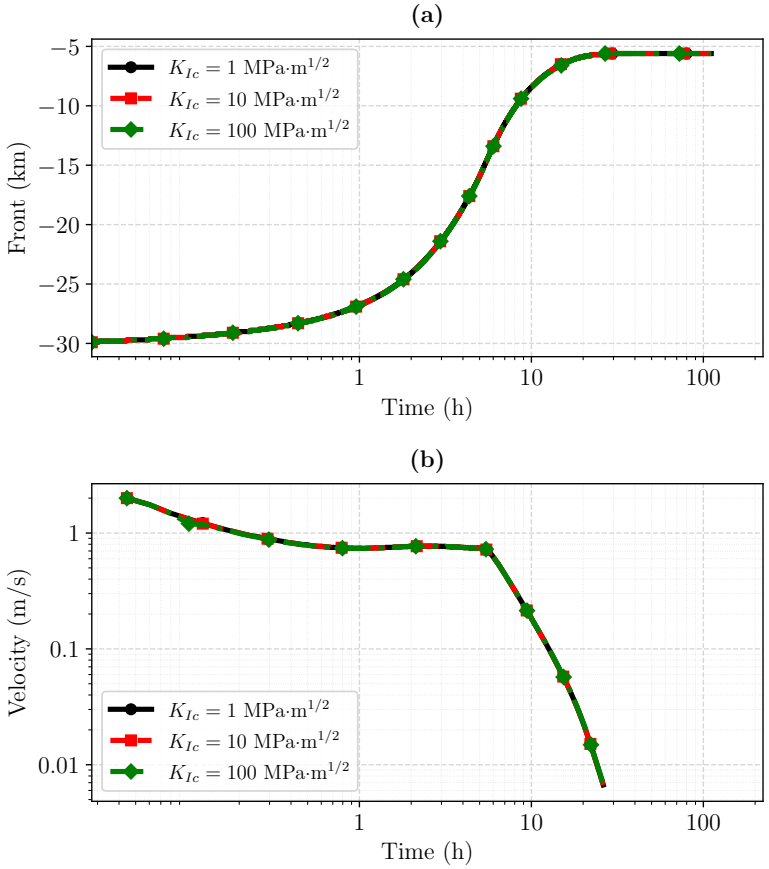

Figure 6. Effect of fracture toughness on dike propagation. (a) Front position over time for three values of fracture toughness K_{Ic} (1, 10, and 100 MPa·m$^{1/2}$). (b) Corresponding ascent velocity on a logarithmic scale. No significant differences are observed, indicating that K_{Ic} has limited influence within this range.

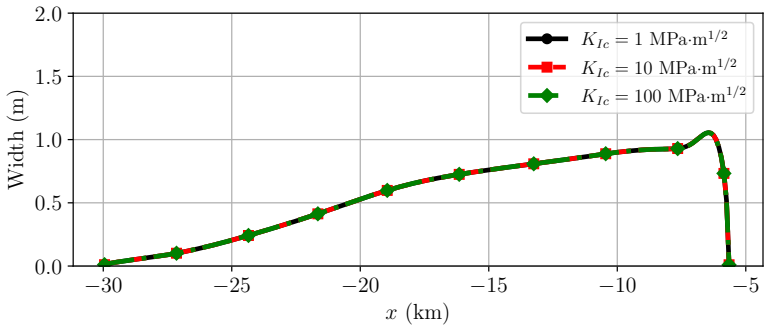

Figure 7. Effect of fracture toughness on dike width at the final time step. Width profiles are nearly identical for all tested K_{Ic} values, confirming the weak sensitivity of the model to fracture toughness in this range.

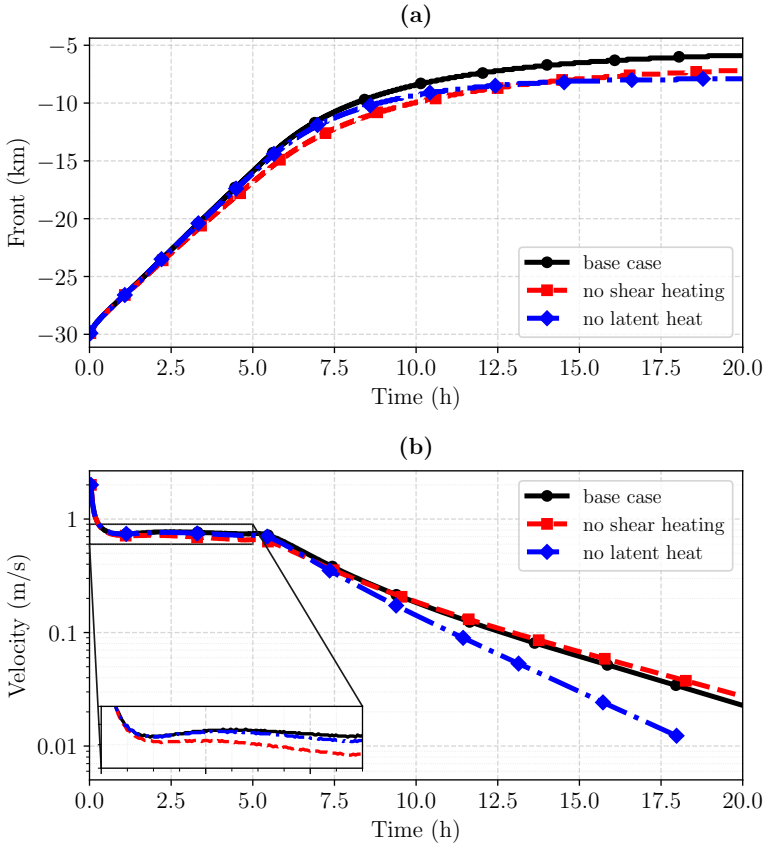

Figure 8. Dike front evolution (a) and ascent velocity (b) for the same cases as in Fig.12 in main text, but shown over a shorter time interval to highlight the distinct roles of shear heating and latent heat.

REFERENCES

Ghiorso, M. S. & Gualda, G. A., 2015. An H2O–CO2 mixed fluid saturation model compatible with rhyolite-MELTS, *Contributions to Mineralogy and Petrology*, **169**, 1–30.

Iacovino, K., Matthews, S., Wieser, P. E., Moore, G., & Bégué, F., 2021. Vesical part i: An open-source thermodynamic model engine for mixed volatile (h2o-co2) solubility in silicate melts, *Earth and Space Science*, **8**(11), e2020EA001584.

Roper, S. & Lister, J., 2007. Buoyancy-driven crack propagation: The limit of large fracture toughness, *Journal of Fluid Mechanics*, **580**, 359–380, doi: 10.1017/S0022112007005472.